Applied Surface Science 256 (2010) 4031–4037

Contents lists available at ScienceDirect

Applied Surface Science

journal homepage: www.elsevier.com/locate/apsusc

Laser smoothing of sub-micron grooves in hydroxyl-rich fused silica

Nan Shen, Manyalibo J. Matthews *, James E. Fair, Jerald A. Britten, Hoang T. Nguyen, Diane Cooke, Selim Elhadj, Steven T. Yang

Lawrence Livermore National Laboratory, 7000 East Avenue, L-491, Livermore, CA 94550-9234, USA

ARTICLE INFO

Article history:
Received 12 November 2009
Received in revised form 20 January 2010
Accepted 21 January 2010
Available online 1 February 2010

Keywords:
Viscosity
Capillarity
Laser polishing
Damage mitigation
Fused silica
Hydroxyl group

ABSTRACT

Nano- to micrometer-sized surface defects on UV-grade fused silica surfaces are known to be effectively smoothed through the use of high-temperature localized CO_2 laser heating, thereby enhancing optical properties. However, the details of the mass transport and the effect of hydroxyl content on the laser smoothing of defective silica at sub-micron length scales are still not completely understood. In this study, we examine the morphological evolution of sub-micron, dry-etched periodic surface structures on type II and type III SiO_2 substrates under 10.6 μm CO_2 laser irradiation using atomic force microscopy (AFM). In situ thermal imaging was used to map the transient temperature field across the heated region, allowing assessment of the T-dependent mass transport mechanisms under different laser-heating conditions. Computational fluid dynamics simulations correlated well with experimental results, and showed that for large effective capillary numbers ($N_c > 2$), surface diffusion is negligible and smoothing is dictated by capillary action, despite the relatively small spatial scales studied here. Extracted viscosity values over 1700–2000 K were higher than the predicted bulk values, but were consistent with the surface depletion of OH groups, which was confirmed using confocal Raman microscopy.

Published by Elsevier B.V.

1. Introduction

Thermal modification of nano- and micro-structures on a wide variety of material surfaces to create or enhance surface properties using long-wave CO_2 lasers has enjoyed significant success in recent decades [1,2]. Recently, localized CO_2 laser heating of silica glass has been successfully applied to control and mitigate surface damage on optics used in high power laser applications such as inertial confinement fusion (ICF) [3–5]. In particular, minimizing damage initiation and shot-to-shot damage growth on UV-grade optic surfaces which have been mechanically polished [6], laser machined [7] or optically damaged [8] is crucial to enhancing overall laser performance. However, the physics of the apparent extrinsic damage threshold of fused silica surfaces is still a subject of debate, and therefore the mechanism by which this threshold is enhanced by CO_2 laser heating is also not completely clear. Because the nano- and micro-scale fractured surfaces associated with polishing/machining are believed to be associated with a higher concentration of UV-absorbing damage precursors [9,10], thermal treatment may act to allow these defects to anneal by way of surface or bulk diffusion. On the other hand, enhancement of local field intensity from irregular interfaces, clearly present on optically damaged and laser machined surfaces, could also act to lower the damage threshold of laser optics [11,12]. In this case, CO_2 laser heating would act to macroscopically smooth these surfaces into more regular interfaces, thus lowering near-field intensification effects. Therefore, the exact role and contribution from each of these mechanisms and the optimization of CO_2 laser surface treatment from a fundamental point of view, remains somewhat unclear. It is of interest therefore to explore the temperature dependence of the reshaping of model surfaces to understand the relative contributions from capillarity and diffusion, as well as influence from structural-chemical changes, to the mitigation of specific defects associated with UV absorption.

Previous theoretical studies of the isothermal relaxation of modulated surfaces under capillary, evaporative and diffusive processes can be traced back to the pioneering work by Mullins nearly four decades ago [13,14]. For an arbitrary surface Fourier decomposed into frequency components $\omega = 2\pi/\lambda$, where λ is the spatial period, the relative importance of each transport process to the time evolution of a nearly-flat surface of height $S(x,y,t)$ can be described by

$$\frac{\partial S}{\partial t} = -(F\omega + A\omega^2 + D\omega^3 + B\omega^4)S \quad (1)$$

where F, A, D, and B are the decay constants for capillary flow, evaporation–condensation, bulk diffusion, and surface diffusion respectively. Although for the relaxation of nanoscale surface features both surface diffusion and viscous flow should be the

* Corresponding author. Present address: 7000 East Avenue, L-592, Livermore, CA 94550, USA. Tel.: +1 925 424 6762; fax: +1 925 422 5099.
E-mail address: ibo@llnl.gov (M.J. Matthews).

0169-4332/$ – see front matter. Published by Elsevier B.V.
doi:10.1016/j.apsusc.2010.01.073

dominant transport processes, Wang et al. [15] recently concluded that, for isothermal heating of sub-micron Al–Ca–Si oxide gratings, the effect of surface diffusion is negligible. One possible explanation the author attributed to the observation is the existence of defects which reduces surface diffusion [16], though the mechanism of surface diffusion on highly defective ceramic surfaces is still poorly understood. A similar, yet somewhat empirical, approach derived for borosilicate thin films [17] was used by Nowak et al. [18] to study laser polishing of micron-scale features in fused silica. A decay function, similar to that in Eq. (1) was used to fit data, but deviation in the expected spatial power scaling was left unresolved. Because laser materials processing of roughened and defective surfaces is subject to a dynamic and non-uniform temperature field, it is not clear what mechanisms are at play, particularly at the relatively shorter time scales and higher transient temperatures characteristic of laser processing.

It is well-known that OH content plays a significant role in determining the thermomechanical properties of fused silica glass, particularly viscosity. For example, in the low water content regime (<0.1 wt%), water exits mainly as structurally bound and immobile hydroxyl groups [19], yielding viscosities (in Poise) of $\log \eta \sim 14$ at 1400 K. In contrast, high water content silica can contain more loosely bound and mobile OH groups and H_2O, leading to viscosities of $\log \eta \sim 12$ at 1400 K. One model developed by Adam and Gibbs [20] to understand the mechanism by which water affects glass melts quantifies the rate of structural relaxation as a function of both kinetic and thermodynamic parameters. The fundamental idea of the model is that the relaxation of a liquid to an equilibrium configuration following a change in external conditions is limited not only by local bond strengths (i.e., Si–O), but also by the number of configurations the liquid can access at any particular temperature, which is enhanced by OH mobility. Therefore, the introduction of different amounts of OH content in silica glass leads to variation in configurationally entropy and the heat capacity of the glass, affecting their viscosity.

In this work, we simulate the process of viscous glass flow using computational fluid dynamics (CFD) software and compare it to the measured decay kinetics of semi-square sub-micron gratings etched on fused silica glass with different OH content. Direct measurement of the transient temperature field and changes in near-surface glass structure and composition is used to estimate the viscosities and relaxation times associated with grating decay. As surmised in previous studies, depletion of OH from the surface, confirmed by Raman microscopy, leads to a shift in viscosity to higher values than predicted for the bulk. However, for large effective capillary numbers, N_c, i.e. shorter time scales (<1 s) and lower temperatures (<1700 K), this shift is less dramatic, and may indicate an enhancement of surface relaxation caused by either surface diffusion or an incomplete near-surface depletion of OH species.

2. Sample preparation and experimental procedure

We used two types of fused silica glass in the study, Corning 7980 (type III, 800–1000 ppm OH content by weight) and Heraeus Suprasil 312 (type II ~200 ppm OH content by weight), which we will refer to as samples C-3 and H-2 respectively. These samples were chosen primarily because of their relatively wide use in UV-grade laser optics, and their disparate OH levels. One-dimensional trapezoidal gratings with a period of ~650 nm and a height of ~700 nm were patterned on 51 mm round, 10 mm thick, silica samples using laser interference lithography and ion-beam etching [21] as shown in Fig. 1. Grating shapes were nearly isosceles, with grating tops ~250 nm wide with RMS roughness of ~1%. Patterned silica samples were exposed to focused CW 10.6 μm CO_2 laser light from a Synrad firestar V20, with a maximum output power of 20 W and power stability of ±5%. The laser beam profile was nearly a

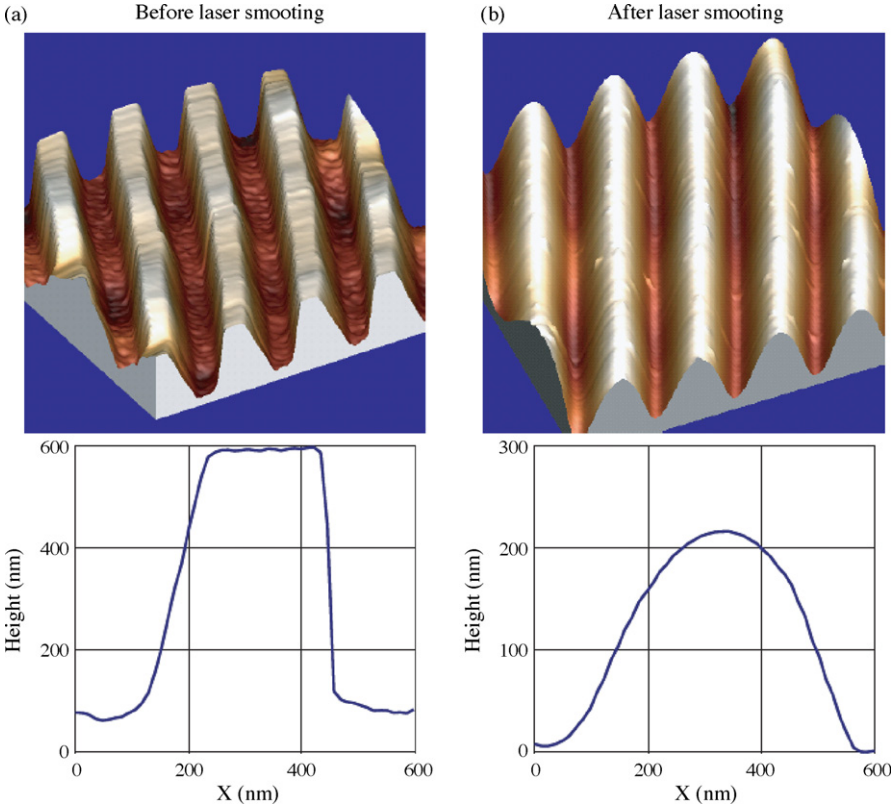

Fig. 1. Typical AFM images of grating (a) before and (b) after CO_2 laser polishing.

perfect Gaussian a $1/e^2$ diameter of ~1 mm, as characterized by a beam profiler (Pyrocam III, Spiricon). The laser power delivered to the sample was set to between 3.8 and 4.7 W, while the exposure time was adjusted from 100 ms to 100 s. This narrow power range was chosen to observe surface relaxation over reasonable experimental time spans, while also staying well below the evaporation threshold of ~3000 K [4]. During each laser exposure, the sample surface temperature was monitored in situ by using a calibrated LN-cooled HgCdTe camera operating at 33 fps, with an optical resolution of ~100 μm (sampled at 40 μm spacing). Although this spatial resolution is quite coarse relative to the grating geometry, it can be shown that, in fact, the calculated temperature profile established by a 1 mm beam varies quite slowly over the length scales studied here. Further details of the laser exposure setup and thermographic analysis can be found in Ref. [22]. The surface morphology of each laser exposed region of the etched samples was characterized before and after exposure using a Digital Instrument Dimension 3100 atomic force microscope (AFM). We used high aspect ratio silicon tips (Veeco OTESPAW) to ensure the accuracy of our AFM results, and to minimize any tip convolution of the shapes measured. Instrument resolution was <1 nm vertically and ~10 nm laterally. Finally, spatially-resolved variations in OH content caused by laser heating were measured using confocal Raman microscopy operating at 532 nm (CW), with a spatial (depth) and spectral resolution of 5 μm and 4 cm^{-1} respectively [23]. Our detection limit of OH content was estimated to be roughly 100 ppm by weight.

3. Simulation of the surface relaxation

The surface evolution of the 2D periodic step during laser heating was simulated using a commercial computational fluid dynamics code optimized for free surface flow [24]. Because our goal was to use the simulation as a basis for comparison with experiment, explicit viscous stress and surface capillary pressure evaluations were used to ensure maximum accuracy of the numerical solution.

Taking as a characteristic velocity $U = W/t$, where W is the grating period, t is the exposure time, and evaluating Reynolds Number N_{Re}, Weber Number N_{We} and Froude Number N_{Fr} ratios using published material constants for fused silica [25] to determine the relative roles of inertial, viscous, capillary and gravitational forces we find all these ratios are $<<1$: $N_{Re} = 2 \times 10^{-15}(1/t)$, $N_{We} = 9 \times 10^{-15}(1/t^2)$, $N_{Re}/(N_{Fr})^2 = 2.2 \times 10^{-8}(t)$, and $N_{We}/(N_{Fr})^2 = 8.6 \times 10^{-8}$. Hence, with typical flow times of 1–100 s and in the non-evaporative regime, only viscous and capillary forces are important in determining surface reshaping and material transport. Unfortunately, this problem resists solution by explicit algorithm because the small spatial scale in conjunction with large shear forces leads to a severe restriction in maximum computational time steps. For example, the maximum computation time step $\Delta t_{\min}$ associated with viscous momentum transport for fused silica at 2000 K given a density $\rho \sim 2.2$ g/cm^3 and a minimum mesh size $\Delta x_{\min} \sim 10$ nm is limited to $\Delta t_{\min} \lesssim ((\rho \Delta x_{\min}^2)/\eta) \sim 10^{-19}$ s, a very impractical value. However, by taking the ratio N_{Re}/N_{We} we can define a non-dimensional relaxation variable τ (the inverse capillary number, N_c^{-1}),

$$\tau \equiv \left(\frac{W^2\rho}{\eta t}\right)\left(\frac{W^3\rho}{\sigma t^2}\right)^{-1} = \frac{\sigma t}{\eta W} = N_c^{-1} \tag{2}$$

and establish the only required equivalence condition of formal dynamic similarity. In Eq. (2), σ is the surface tension of fused silica which has a relatively weak temperature dependence compared to that of the viscosity [26]. We are therefore free in the numerical simulation to uniformly reduce surface tension and viscosity without influencing the essential character of the system. The only restriction is that we not decrease viscosity to the point where

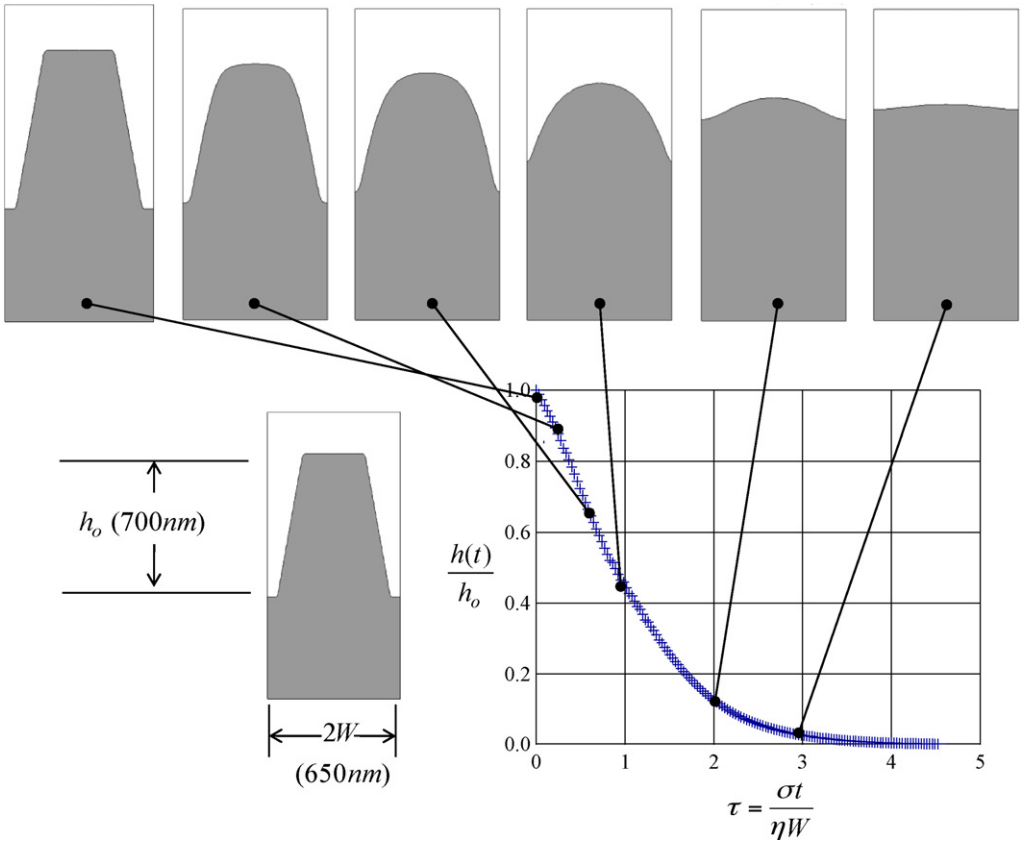

Fig. 2. Simulated grating height evolution with analytical fit.

Table 1
Function parameters used to approximate viscous relaxation behavior.

	C	K	M
$\tau < 2$	1.00	0.80	1.35
$\tau > 2$	3.14	1.57	1.00

inertial effects become appreciable, because as previously established, inertia plays no significant role in this problem. This practical constraint is simply that N_{Re} in the simulation remain below approximately 0.01.

The flow of a periodic surface structure closely approximating those formed by photolithography (Fig. 1) for our study was simulated. Taking advantage of the inherent symmetry, only one half of the periodic structure was included in the calculation. A uniform 10 nm finite difference grid was used with 90° free surface contact angle constraints and free-slip, zero flux conditions imposed at domain boundaries. The simulation was performed using constant (local) viscosity and surface tension, consistent with $W \ll l_{th}$ where $l_{th} \sim 1$ mm is the thermal diffusion length. The model geometry and results of the simulation are shown in Fig. 2, indicating snapshots of the surface profile as it evolves during the surface tension driven flow process. As shown, the surface assumes a sinusoidal profile at a dimensionless time between $\tau = 1$ and $\tau = 2$. It is evident that pure exponential decay of the step height commences around $\tau = 2$. The early time behavior is consistent with the findings of Cassidy and Gjostein [27] who analyzed similar idealized flat top structures by the phenomenological theory of Mullins [13] based on Fourier decomposition of the surface profile into a set of independent decay modes. The long time behavior follows simple exponential decay corresponding to viscous relaxation of a pure sinusoidal surface under forces of capillary pressure [17]. Therefore, the time evolution of grating height $h(t)$ from an initial height h_0 can be reasonably approximated in these two regimes using two analytic functions of the form

$$\frac{h(t)}{h_0} = C\exp(K\tau^M) \tag{3}$$

where the parameters C, K, M for small ($\tau < 2$) and large ($\tau > 2$) values of τ are given in Table 1. These analytic functions could then be used to directly fit experimental surface height data corresponding to surface treatments at varying temperatures and times.

4. Results

Due to the non-uniform heating inherent to laser materials processing, the spatial profile of the laser power translates into a variation in surface temperature resulting in an effective viscosity profile (Fig. 3). The resulting spatial non-uniformity in flow dynamics was probed by measuring the height change of the grating at different locations within one laser beam, and correlating each spatial subset of data with in situ surface temperature measurements. Fig. 3a shows a microscope image of sample C-3 treated with a 3.8 W, 100 s exposure, with square boxes indicating radial sub-regions that were scanned using AFM. For comparison, the Gaussian laser beam profile and the resulted spatial distribution of grating heights were illustrated with schematics in Fig. 3a. High-resolution AFM scans along the radius of the exposed regions separated by 25 μm were taken for each case studied, as shown in the upper graph of Fig. 3b. Simultaneous to the laser exposure, 2D thermographic images were taken using the HgCdTe camera, which could be spatially registered with subsequent AFM scans, as indicated by the temperature profile shown in the lower panel of Fig. 3b. The peak on-axis temperature ranged from 1140 to 1640 K and 1340 to 1960 K for the 3.8 and 4.7 W exposures respectively, with the temperature rise scaling with exposure time 100 ms $< t <$ 100 s roughly as $\sqrt{t}$. Although the steady-state temperature profile is known to vary as a Bessel-weighted Gaussian [28], near the peak we use a simple Gaussian fit to extract the temperature variation, as indicated in Fig. 3b.

As described in Section 3, the surface flow dynamics are expected to depend principally on the viscosity, which, for a wide range of glasses and temperatures follows the so-called Vogel–Fulcher–Tammann (VFT) expression [29],

$$\eta = \eta_0 \exp\left(\frac{B_0}{T - T_0}\right) \tag{4}$$

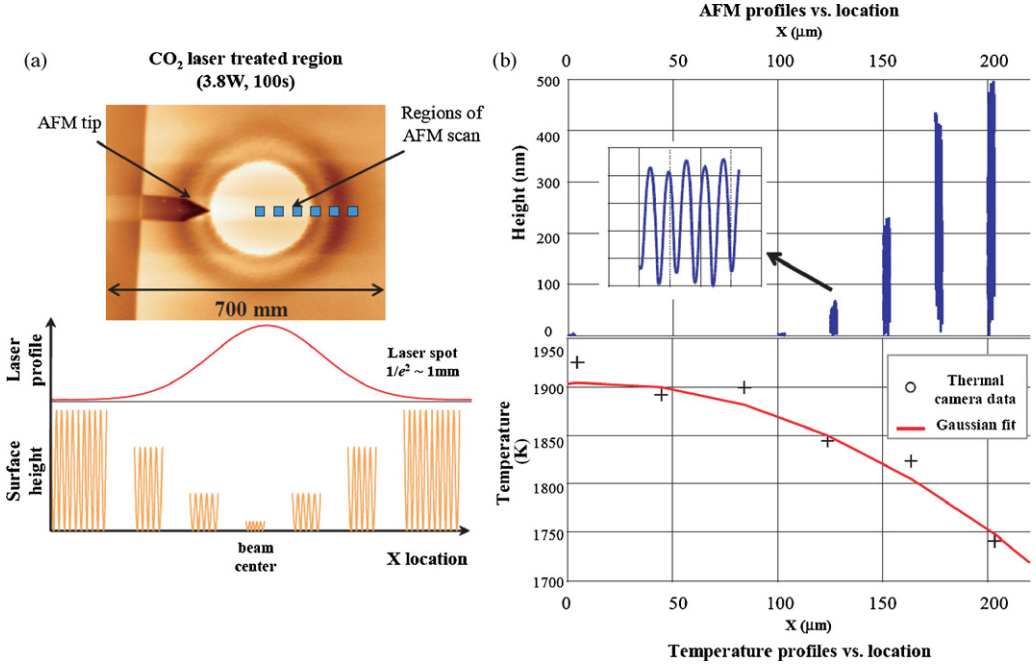

Fig. 3. Spatial map of the region where surface profiles of the grating were measured using AFM and the corresponding temperature at that location. (a) Microscopy image of region treated with the Gaussian CO_2 laser beam and (b) the grating height at different locations relative to laser beam center and the in situ temperature measurement.

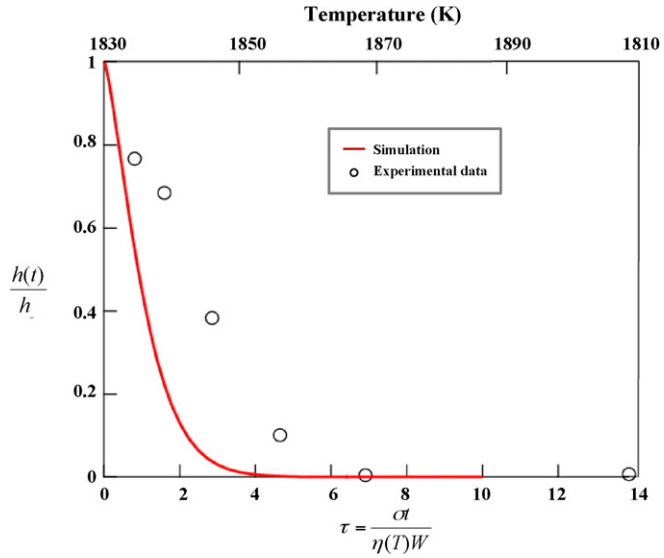

Fig. 4. Experiential (open circle) and simulation (straight line) results of normalized grating height vs. τ. The values of τ were calculated using Arrhenius relation $\eta = \eta_0 \exp(E_a/RT)$ for the literature reported viscosity for silica glasses with ~1100 OH content where $\eta_0 = 8.81 \times 10^{-5}$ Poise and $E_a = 434$ kJ/mole.

where η_0, B_0 and T_0 are temperature-independent constants. However, since we are studying the behavior of glass flow in a relatively narrow temperature range (1700–2000 K), the VFT equation can be well-approximated by an Arrhenius relation, $\eta = \eta_0 \exp(E_a/RT)$, where E_a is the activation energy of viscous glass flow and R is the gas constant. The values of η_0 and E_a have been reviewed and summarized for a wide range of OH containing SiO_2 samples by Zandian et al. [30]. The C-3 sample is a type III glass containing ~1000 ppm OH corresponding to a reported value of $\eta_0 = 8.81 \times 10^{-5}$ Poise and $E_a = 434$ kJ/mole. Applying these values into our expression for viscosity for the 3.8 W, 100 s exposure condition and comparing it with our CFD simulation, a significant discrepancy was found between simulation and experiment (Fig. 4). In the experiment, since the laser exposure time and local surface temperature are known for each sub-region studied within the treated regions, measurement of the grating morphology changes can, in fact, be used to estimate local viscosity [27]. By inserting the aforementioned Arrhenius approximation for viscosity into the expression for τ (Eq. (2)), and fitting $h(t)/h_0$ as a function of T for a single case (3.8 W/100 s), we could obtain η_0 and E_a for sample C-3 under CO_2 laser polishing conditions (Fig. 5a). Using the same approach, we also calculated η_0 and E_a for sample H-2 (Fig. 5b). Table 2 summarizes the values of the activation energy for the two types of silica glass found in the literature and measured under our experimental conditions. The extracted viscosity was then applied to all laser exposure conditions for sample C-3 and H-2. A reasonable agreement between the experiment and simulation is achieved with several different laser parameters when we used this new Arrhenius expression for viscosity (Fig. 6). However, for small τ (short exposure times and lower temperatures), there existed a deviation in the data away from the curve indicating a faster relative decay rate.

Table 2
Viscous flow activation energies for different fused silica glass samples.

Sample	Arrhenius fitting parameters		Reported value	
	Pre-exponential	Activation energy (kJ/mole)	Pre-exponential	Activation energy (kJ/mole)
Corning 7980	3×10^{-9}	603	8.81×10^{-5}	434
Suprasil 312	2.05×10^{-8}	578	5.8×10^{-7}	515

5. Discussion

For capillary-driven flow, viscosity limits the relaxation processes near glass transition temperature. Therefore knowing the viscosity of a glass is important to predicting processing results. Direct measurement of the viscosity of glass at high temperature is often difficult, especially under extreme, non-uniform conditions such as CO_2 laser mitigation. Study of the relaxation of grating structures may provide an attractive method to indirectly fine-tune the temperature dependant viscosity at high temperature. It is worth noting that the non-dimensional parameter τ gives some insight on the relationship between time and viscosity (temperature) during laser polishing. When designing methods for polishing a feature of size W, it is possible to achieve smoothing by optimizing either the transient exposure time t or temperature to reach a desired viscosity.

Although we simplified the problem of surface relaxation by considering only the heat activated surface tension driven mass flow, the model adequately describes the CO_2 laser smoothing of sub-micron sized SiO_2 gratings for most of the temperature/time scales examined here. The computational fluid dynamics simulation based on this model afforded us the ability to treat exactly realistic (e.g. trapezoidal) gratings of any aspect ratio, without the constraints typical of the nearly-flat plane solution [13,27]. In particular, deviation from a pure exponential decay can be observed due to relaxation of higher spatial frequency components. For example, the

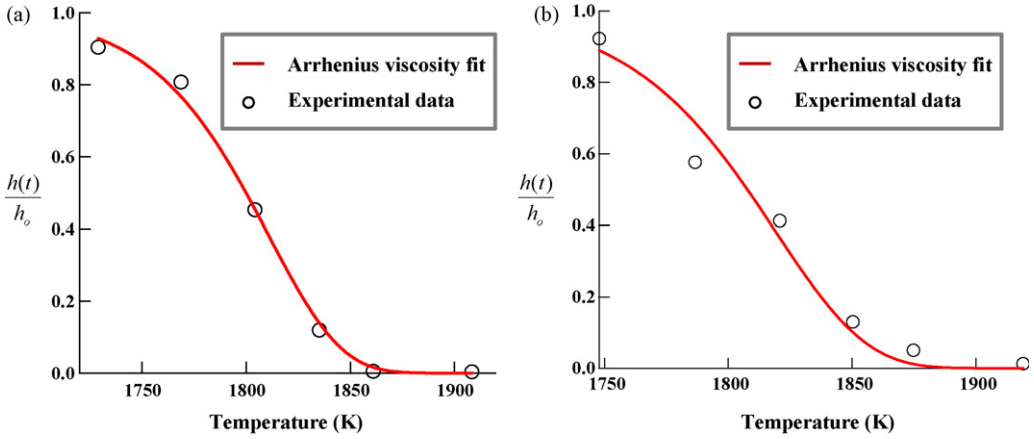

Fig. 5. Arrhenius temperature dependent viscosity relation $\eta = \eta_0 \exp(E_a/RT)$ obtained by fitting experiment data for (a) type III (C-3) and (b) type II (H-2) silica glasses.

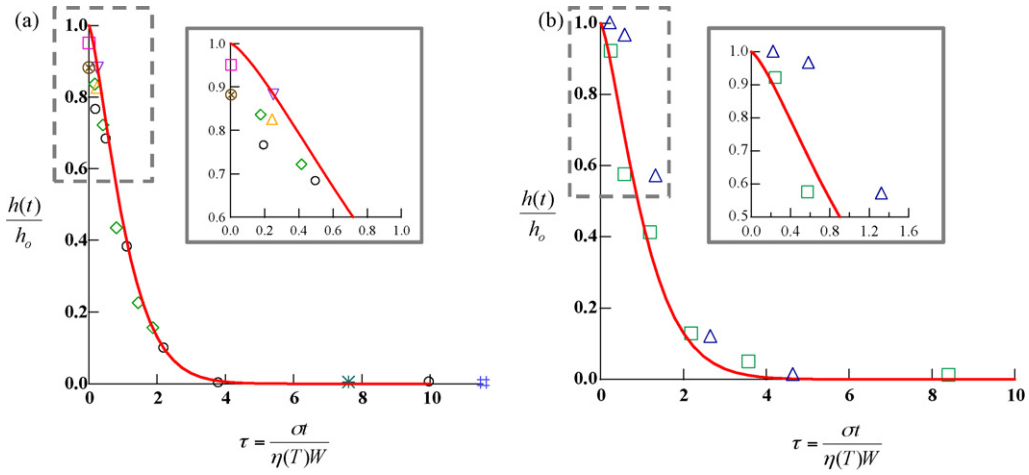

Fig. 6. Experimental (open symbols) and simulation (solid line) of the evolution of the grating height vs. τ. For (a) type III (C-3), the laser parameters are 3.8 W 10 s (□), 3.8 W 100 s (○), 4 W 100 s (✳), 4.2 W 10 s (▽), 4.5 W 5 s (△), 4.5 W 30 s (#), 4.7 W 1 s (⊕) and 4.7 W 10 s (◇). For (b) type II (H-2) silica glass, the laser parameters are 3.8 W 10 s (□), 4.5 W 10 s (△).

spatial power scaling M shown in Table 2 was found to be 1–1.35 for our geometry, similar to the values found by Nowak et al. for larger scale surface features [18]. It is important to point out that, although a power scaling $M > 1$ might imply the contribution of other mechanisms through Eq. (1), capillary flow of high aspect ratio, non-sinusoidal geometries leads to a similar effect.

A key consideration here with regard to capillarity is the proper temperature dependent viscosity, which for silica is strongly dependent on OH content [30]. The viscosity extracted from our simulation and experiments for both high and low OH samples for τ larger than ~0.5 ($N_c < 2$) indicated a shift in E_a towards higher values. The higher activation energy E_a could suggest that the hydroxyl content may have diffused out during laser heating. The apparent increase in viscosity due to an assumed OH diffusion was reported by Wang et al., and though highly plausible, only bulk OH was actually measured [15]. Indeed, given the smaller starting OH content, it is interesting to note that the viscosity shift for the lower OH sample (H-2) was somewhat less. In order to explore laser heating-induced chemical changes that may correspond to higher activation energies estimated from our surface smoothing results, we performed spatially-resolved confocal Raman microscopy to monitor the OH variation on the sample surface and in bulk. The normalized intensity of the SiOH stretch at ~3700 cm^{-1} has been shown to give a reasonable estimate of the amount of OH [23], given the spectra can be calibrated with a known OH sample. Bulk infrared transmission measurements of sample H-2 were performed by the vendor [31] and used to calibrate OH changes detected by Raman for both samples. Fig. 7 shows the OH variation as a function of depth (axial resolution ~5 μm) for each sample type, for different exposure times. The estimated bulk OH content ~900 ppm for sample C-3 was consistent with quoted vendor specs (800–1000 ppm). As shown, a clear OH depletion region is evident for sample C-3, consistent with the relative increase in viscosity predicted by our relaxation analysis. As expected, when exposure time is decreased from 100 to 1 s, less OH is depleted from the C-3 sample, a ~200 ppm decrease as opposed to ~400 ppm. On the other hand, the H-2 sample showed much less of an effect, though the low starting OH content and relative sensitivity of our measurement (~100 ppm) may limit our ability to assess OH depletion for this sample. It is interesting to note that the variation in the OH content of sample C-3 at the surface for different laser parameters may explain some of the scatter in h/h_0 vs. τ below $\tau = 0.5$ shown in Fig. 4: while the viscosity was estimated using a heavily depleted case ($t = 100$ s), shorter times may retain more bulk-like OH levels and hence viscosity closer to that of the bulk. On the other hand, a stronger decay of h/h_0 could also point to a possible contribution from surface diffusion, not accounted for in our model. Although this deviation was not as strong in sample H-2, thus supporting a possible non-uniform OH effect, further studies are planned to elucidate this apparent discrepancy for small τ in high OH samples.

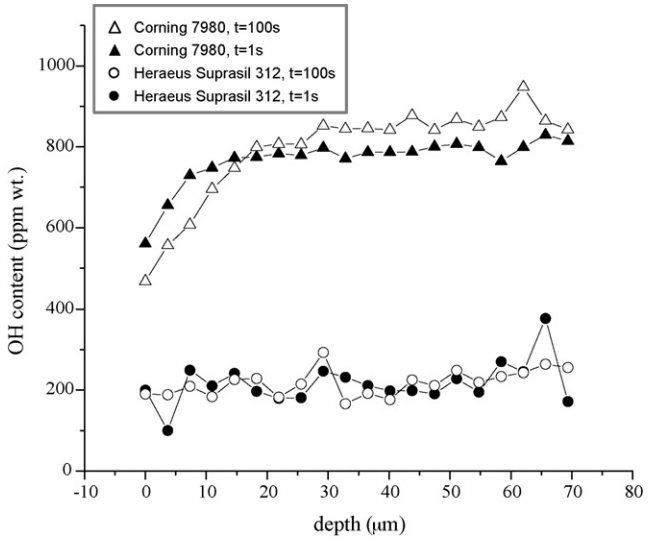

Fig. 7. Measured OH concentration for samples C-3 (triangles) and H-2 (circles) as a function of depth and for 1 s (closed symbols) and 100 s (open symbols) exposures.

6. Conclusions

The smoothing of nanometer-scale, dry-etched periodic surface structures on type II and type III SiO_2 substrates with 10.6 μm CO_2 laser has been studied using atomic force microscopy (AFM). In situ thermal imaging was used to map the transient temperature field across the heated region, allowing assessment of the T-dependent mass transport mechanisms and surface reshaping under different laser-heating conditions. Computational fluid dynamics simulations correlated well with experimental results, and showed that capillary-driven flow dominates, even at the relatively small spatial scales studied here. The transient local viscosity of the silica glass appears to deviate from typical literature values, consistent with a

depletion of OH content that varies with exposure conditions. However, at shorter time scales (<1 s) and lower temperatures (<1700 K), this shift is less dramatic, and may indicate an enhancement of surface relaxation caused by either surface diffusion or an incomplete near-surface depletion of OH species.

Direct measurement of the OH content using micro-Raman confirmed these general conclusions, though the possible influence of surface diffusion in altering relaxation behavior remains somewhat unclear and is a subject of future study.

Acknowledgements

The authors would like to thank Drs. Bill Henshaw and Michael Feit for useful discussions on UV light scattering, and Dr. James Stolken for help in assessing silica viscosity data. This work performed under the auspices of the U.S. Department of Energy by Lawrence Livermore National Laboratory under Contract DE-AC52-07NA27344.

References

[1] W.W. Duley, CO_2 Lasers, Effects and Applications, Academic, New York, 1976.
[2] N.B. Dahotre, Lasers in Surface Engineering, ASM International, Materials Park, OH, 1998.
[3] I.L. Bass, V.G. Draggoo, G.M. Guss, R.P. Hackel, M.A. Norton, Conference on High-Power Laser Ablation VI, Taos, NM, (2006), p. A2612.
[4] E. Mendez, K.M. Nowak, H.J. Baker, F.J. Villarreal, D.R. Hall, Appl. Opt. 45 (2006) 5358–5367.
[5] S. Palmier, L. Gallais, M. Commandre, P. Cormont, R. Courchinoux, L. Lamaignere, J.L. Rullier, P. Legros, Appl. Surf. Sci. 255 (2009) 5532–5536.
[6] J.H. Campbell, Glass Sci. Technol. 75 (2002) 91–108.
[7] R.R. Prasad, J.R. Bruere, J. Peterson, J. Halpin, M. Borden, R.P. Hackel, Laser-Induced Damage in Optical Materials: 2003, vol. 5273, 2003, 288–295.
[8] S.G. Demos, M. Staggs, M.R. Kozlowski, Appl. Opt. 41 (2002) 3628–3633.
[9] L. Gallais, J.Y. Natoli, C. Amra, Opt. Expr. 10 (2002) 1465–1474.
[10] T.A. Laurence, J.D. Bude, N. Shen, T. Feldman, P.E. Miller, W.A. Steele, T. Suratwala, Appl. Phys. Lett. 94 (2009) 151114–151116.
[11] F.Y. Genin, A. Salleo, T.V. Pistor, L.L. Chase, J. Opt. Soc. Am. A: Opt. Image Sci. Vis. 18 (2001) 2607–2616.
[12] D.B. Ge, X.Q. Zhu, 8th World Multi-Conference on Systemics Cybernetics and Informatics, Orlando, FL, (2004), pp. 49–52.
[13] W.W. Mullins, J. Appl. Phys. 30 (1959) 77–83.
[14] W.W. Mullins, J. Appl. Phys. 28 (1957) 333–339.
[15] L.L. Wang, A.J.G. Ellison, D.G. Ast, J. Appl. Phys. 101 (2007).
[16] A.G. Naumovets, Physica A 357 (2005) 189–215.
[17] L.K. White, N.A. Miszkowski, W.A. Kurylo, J.M. Shaw, J. Electrochem. Soc. 139 (1992) 822–826.
[18] K.M. Nowak, H.J. Baker, D.R. Hall, Appl. Opt. 45 (2006) 162–171.
[19] M.J. Davis, Geochim. Cosmochim. Acta. 63 (1999) 167–173.
[20] G. Adam, J.H. Gibbs, J Chem Phys. 43 (1965) 139–146.
[21] J.A. Britten, W. Molander, A.M. Komashko, C.P.J. Barty, 35th Annual Symposium on Optical Materials for High-Power Lasers, Boulder, CO, (2003), pp. 1–7.
[22] S.T. Yang, M.J. Matthews, S. Elhadj, J. Appl. Phys. 106 (2009) 1031061–1031067.
[23] J.C. Mikkelsen, F.L. Galeener, W.J. Mosby, J. Electron Mater. 10 (1981) 631–651.
[24] C.W. Hirt, Flow3D^{TM} V9.3 Flow Science, Inc., 2009.
[25] R. Bruckner, J. Non-Cryst. Solids 5 (1970) 123–175.
[26] N.M. Parikh, J. Am. Ceram. Soc. 41 (1958) 18–22.
[27] D.C. Cassidy, N.A. Gjostein, J. Am. Ceram. Soc. 53 (1970) 161.
[28] M. Lax, J. Appl. Phys. 48 (1977) 3919–3924.
[29] R.H. Doremus, J. Appl. Phys. 92 (2002) 7619–7629.
[30] V. Zandian, J.S. Florry, D. Taylor, Br. Ceram. Trans. J. 90 (1991) 59–60.
[31] Heraeus, private communication.